Pergamon

Int. J. Heat Mass Transfer. Vol. 40, No. 4, pp. 915–929, 1997

0017-9310/97 $17.00 + 0.00

PII: S0017-9310(96)00120-2

Effects of wall conduction, internal heat sources and an internal baffle on natural convection heat transfer in a rectangular enclosure

Y. S. SUN

Advanced Package Development, Advanced Semiconductor Engineering Inc., Kaohsiung, Taiwan, Republic of China

and

A. F. EMERY

Department of Mechanical Engineering, University of Washington, Seattle, WA 98105, U.S.A.

(*Received* 25 *October* 1995 *and in final form* 29 *March* 1996)

Abstract—Conjugate natural convection heat transfer in a two-dimensional, air-filled enclosure containing discrete internal heat sources and an internal baffle is examined. The enclosure formed of finite conductive walls is designed to simulate the behavior of an experimental window calorimeter in order to correct for losses from the calorimeter. The equations are solved using a finite-volume method for a wide range of Rayleigh numbers, internal–external heat source ratios, solid–fluid conductivity ratios and baffle heights. The influences on the heat transfer and the flow characteristics resulting from the internal heat sources as well as the conductive baffle are discussed. Measurements of temperature distributions in the window calorimeter are also reported. The comparison between numerical predictions and experimental measurements shows that it is inappropriate to specify simple boundary conditions on the window surface of the calorimeter and to neglect the conduction through the baffle, window, and walls. A modified procedure for calculating the temperature distributions on the window surface improves the predicted results and yields good agreement with the measured data. Copyright © 1996 Elsevier Science Ltd.

INTRODUCTION

The present investigation is a detailed study of the coupled conduction and natural convection process in a window calorimeter. The calorimeter is equipped with a heater, a temperature sensor and a baffle. The baffle prevents nocturnal cooling of the sensor and straightens the flow over the glazing. The window calorimeter is represented as a two-dimensional, air-filled rectangular cavity with finite conductive walls, several discrete internal heat sources and an internal baffle (Fig. 1). In operation, a set of resistance wires, the discrete sources, dissipate sufficient heat to keep the temperature measured by the sensors equal to the temperature in the room, T_H. Ideally, if the air in the calorimeter were isothermal and at T_H, no heat would be conducted through the calorimeter walls and all of the heat dissipated by the heater would transfer through the window, thus permitting the calculation of the window U-value, $U = Q/A/(T_H - T)$. In reality, the calorimeter air is not isothermal and corrections have to be made for the heat lost to the room and for the effect of the baffle. The calorimeter analyzed in this study was used to compute the U value of special different window assemblies: single, double, triple glazing; wooden sash, aluminum frames, aluminum frames with a thermal break. When the results were analyzed [1], the computed U values were generally as expected, but at times some of the better insulated windows assemblies performed poorer than the apparently less insulated assemblies. Our initial thought was that the baffle caused the variation, but an analysis by Sun and Emery [2] indicated that it could not account for all of the discrepancy. Some preliminary analysis suggested that the variation was due to heat lost through the insulated walls, and to a non-uniform thermal condition on the outer surface of the window. This study reveals that it is primarily the non-uniform window boundary condition which causes the unexpected variation.

A benchmark study of a square cavity with differentially heated vertical walls and insulated horizontal walls was given by de Vahl Davis [3]. Chenoweth and Paolucci [4] conducted a seminal study of the Boussinesq assumption. Henks and Hoogendoorn [5] examined the stability for air in this benchmark cavity. Recently, increased interest in the study of natural convection in cavities lies in the thermal control of electronic equipment. A number of studies on convection cooling applicable to thermal control of electronic equipment were reviewed by Incropera [6]. Several investigations of convection from discrete heat

NOMENCLATURE

C_p	constant pressure specific heat	β	thermal expansion coefficient [K^{-1}]
g	gravitational acceleration [m s^{-2}]	Γ	diffusion coefficient
h	dimensionless height	κ	conductivity coefficient
H	dimensionless height of cavity	η	heat transfer fraction (=heat transfer through hot wall/total heat transfer)
k	thermal conductivity [W mC^{-1}]	ν	kinematic viscosity [m^2 s^{-1}]
k^*	solid–fluid thermal conductivity ratio ($=k_s/k_f$)	θ	dimensionless temperature
Nu	Nusselt number	τ	dimensionless time
P	dimensionless pressure	ρ	density [kg m^{-3}]
Pr	Prandtl number ($=\nu/\alpha$)	ξ	void fraction ($=hw/HW$).
Ra_E	external Rayleigh number ($=g\beta\Delta TL_0^3/\alpha\nu$)		
Ra_i	internal Rayleigh number ($=g\beta QL_0^5/\alpha\nu k$)		
Q	uniform volumetric heat generation [W m^{-3}]	Subscripts	
q	dimensionless heat transfer rate	b	baffle
U, V	dimensionless velocities	C	cold side
X, Y	space coordinates	f	fluid
W	dimensionless width of cavity.	H	hot side
		h	heater
		s	solid
Greek symbols		S	sensor
α	thermal diffusivity [m^2 s^{-1}]	∞	external.

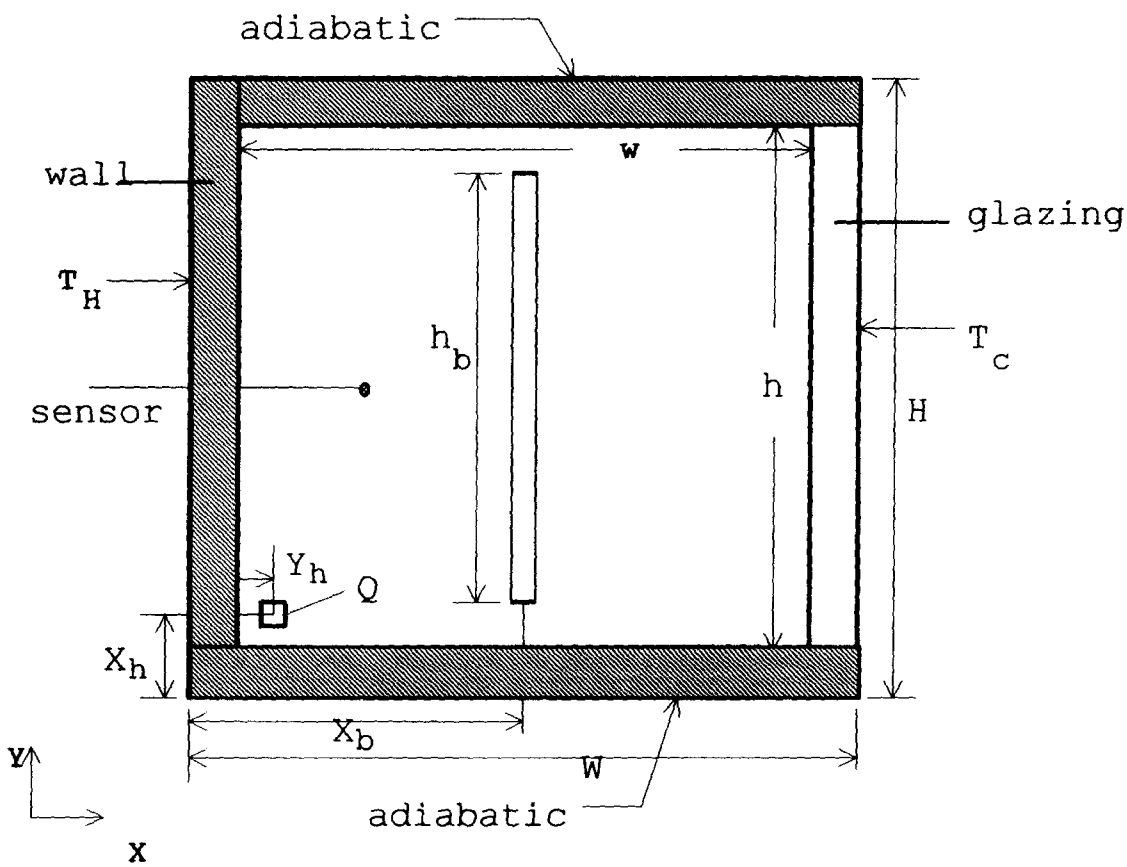

Fig. 1. Model of the experimental system Window Calorimeter.

sources in air have been reported. Acharya and Goldstein [7] computationally examined the heat transfer characteristics in an externally heated vertical or inclined square cavity with uniformly distributed internal energy sources. Conjugate heat transfer for developing flow over finite heat sources on a parallel plate was reported by Davalath and Bayazitoglu [8]. Afrid and Zebib [9] considered heat conduction coupled with convection in air with heat sources protruding from adiabatic vertical surfaces. Discrete heat sources flush mounted on a substrate in a liquid-filled square enclosure were investigated by Joshi *et al.* [10]. However, most of the studies have neglected the interaction between convection in a fluid-filled cavity and conduction in the walls surrounding the cavity. Kim and Viskanta [11] reported the effect of wall heat conduction on natural convection heat transfer in a square cavity without internal heat sources.

ANALYSIS

Physical model and assumptions

The physical model and coordinate system of the problem are illustrated schematically in Fig. 1. The two-dimensional, rectangular cavity is formed by finite conductive walls. A conductive baffle of the same material as the wall and a discrete heat source are mounted inside the cavity. The horizontal walls forming the enclosure are assumed to be insulated externally. Different temperatures are imposed on the outside of the two vertical walls and the properties of the walls and the fluid are taken at the mean temperature. The internal flow is assumed to be steady, laminar, Newtonian and incompressible, the Boussinesq approximation is also valid. A problem with an internal heat source is that the volumetric heat source induces heat transfer and flow characteristics which differ from those of an externally heated cavity, therefore, one extra nondimensional parameter, Ra_I, has to be defined. This new parameter is called the 'internal Rayleigh number'. The Rayleigh number based on the external temperature difference is referred to as the external Rayleigh number, Ra_E,

$$Ra_I = \frac{g\beta Q L_0^5}{\alpha \nu k} \quad \text{and} \quad Ra_E = \frac{g\beta \Delta\theta L_0^3}{\alpha \nu}.$$

The natural convection in this complex configuration can be described by the following set of dimensionless equations:

$$\frac{\partial U}{\partial X} + \frac{\partial V}{\partial Y} = 0 \tag{1}$$

$$\frac{\partial U}{\partial \tau} + U\frac{\partial U}{\partial X} + V\frac{\partial U}{\partial Y} \frac{\partial P}{\partial X} + \frac{\partial}{\partial X}\left(\Gamma \frac{\partial U}{\partial X}\right) + \frac{\partial}{\partial Y}\left(\Gamma \frac{\partial U}{\partial Y}\right) \tag{2}$$

$$\frac{\partial V}{\partial \tau} + U\frac{\partial V}{\partial X} + V\frac{\partial V}{\partial Y} - \frac{\partial P}{\partial Y} + \frac{\partial}{\partial X}\left(\Gamma \frac{\partial V}{\partial X}\right) + \frac{\partial}{\partial Y}\left(\Gamma \frac{\partial V}{\partial Y}\right) + \frac{Ra}{Pr}\theta \tag{3}$$

$$\frac{\partial \theta}{\partial \tau} + U\frac{\partial \theta}{\partial X} + V\frac{\partial \theta}{\partial Y} \frac{\partial}{\partial X}\left(\frac{\kappa}{Pr}\frac{\partial \theta}{\partial X}\right) + \frac{\partial}{\partial Y}\left(\frac{\kappa}{Pr}\frac{\partial \theta}{\partial Y}\right) + \frac{Ra_I}{Ra_E Pr}\theta. \tag{4}$$

The Ra_I/Ra_E term in equation (4) is equal to $QL^2/k\Delta T$, a dimensionless quantity, that is an independent parameter representing the strength of the internal heating. The same set of equations can be applied to the solid portions by using a harmonic-mean formulation in the diffusivities (Γ and κ) for the solid–fluid interfaces. Γ is a general diffusion coefficient which is equal to 1 in the fluid region and 10^{15} in the solid region. By using these values, the velocities automatically approach zero in the solid regions. κ is a general conductivity coefficient which is equal to 1 in the fluid region, and equal to k^* in the solid region, where k^* is the ratio of solid–fluid conductivity. This conjugate approach is very convenient, but it is inefficient because it requires solution of the momentum equations in the area defined by solid materials.

Numerical procedure

Equations (1)–(4) are solved by a control-volume-based finite difference procedure. The equations are expressed in an integral form over each control volume and discretizations are made to represent the interface values and the derivatives in terms of grid point values. Hybrid [12] and QUICKE [13] schemes are employed to obtain the solutions. The results from these two schemes agree reasonably well for small Rayleigh numbers, but differ at higher Rayleigh number flows [14]. Therefore, the second order QUICKE scheme was employed to discretize the convective terms. The velocity–pressure interlinkage was solved using the SIMPLE algorithm [12] and the discretized equations were solved iteratively using a line-by-line TDMA (tri-diagonal matrix algorithm) procedure. The false-time-step method, in which the solution of the steady-state results are found by solving the unsteady equations, was used to stabilize the relaxation procedure.

A non-uniform mesh with a large concentration of nodes in regions of steep gradients, such as close to the solid portions, is employed. The computations were generally performed on a 50×50 mesh with an acceptable grid independence [2]. Convergence was assumed when the L_2 residual norm of major variables was no more than 0.001% per step. The conservation of energy was satisfied; in the worst case the error was no more than 1%. The computational time on a VMS/VAX-6530 computer ranged from 25 to 40 CPU

min depending upon the internal and external Rayleigh numbers.

COMPUTATIONAL RESULTS

The dimensionless parameters that must be specified for the system are: Ra_E, Ra_I, Pr, k^*, the location of the heat source, X_h, the location of the baffle, X_b, the height of the baffle, h_b and the void fraction, ξ, which is defined as the ratio of the fluid area to the area of the entire cavity. Since so many basic dimensionless parameters are required to characterize the system, a comprehensive analysis of all combinations of these parameters is not practical. The numerical results will be aimed at a small fraction of the possible situations, and will explain the effect of several critical parameters in the experimental calorimeter by simplifying the configuration.

Effect of conductive walls

In order to investigate the effect of the conductive walls (void fraction and conductivity ratio), the internal baffle and heat source of Fig. 1 are neglected. Figure 2 shows the variation of the average Nusselt number for different void fractions and conductivity ratios. As the external Rayleigh number increases, the average Nusselt number increases. For the larger thermal conductivity ratios k^*, the heat transfer rate is higher through the wall than the fluid, due to a larger temperature gradient at the solid–fluid interface. The fluid in the cavity behaves as an insulator for a wall of such large thermal conductivity, but, for a small thermal conductivity enclosure, the heat transfer through the solid is lower than in the fluid. Therefore, for a lower conductivity ratio ($k^* = 1$), an increase in void fraction causes an increase in the average Nusselt number. For a higher conductivity ratio ($k^* = 100$), the average Nusselt number decreases with an increase in the void fraction. For a mild conductivity ratio ($k^* = 10$), the effect of the void fraction is not significant for a moderate Rayleigh number ($Ra = 10^6$), since the effects from the wall conduction and the fluid convection almost compensate each other. The average Nusselt number continuously increases for a higher Rayleigh number (10^7) but decreases for a lower Rayleigh number (10^5) when the void fraction increases. Note that the decrease continues even when the void fraction falls below 0.5. These results show that increasing the thickness of a low conductivity wall can reduce the heat loss through the walls, but that the effect becomes marginal when the thickness reaches a certain small value which depends on the conductivity. For highly conductive walls, the thinner the wall is, the less heat transfers through it, with a consequent very strong reduction in Nu.

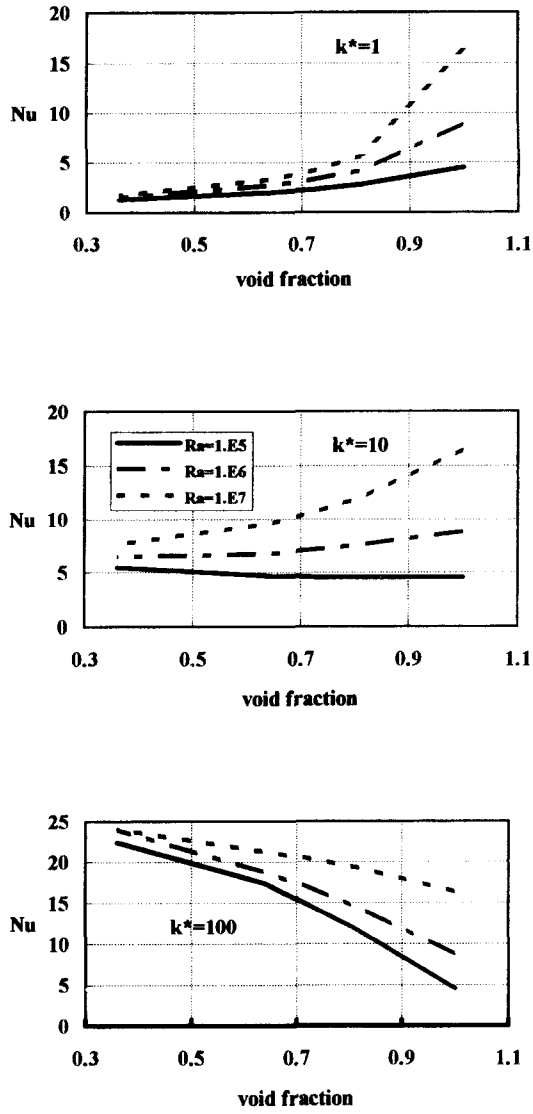

Fig. 2. Effect of void fraction and wall conduction on average Nusselt number.

Effects of internal heat sources

To consider only the effect of a heat source located at the lower left corner of the cavity, the void faction is set to one and the baffle in Fig. 1 is neglected. In the presence of internal heating ($Ra_I > 0$), the trends in the flow and heat transfer of the standard benchmark solutions (without internal heating [3]) persist if $Ra_I/Ra_E < 1$ (Fig. 3a).

For $Ra_I/Ra_E \gg 1$, the internal heater causes the fluid to rise along the hot wall and then to turn into the central region of the enclosure. The flow then moves down both the hot and cold surfaces (Fig. 3c). The flow adjacent to the upper part of the hot wall is directed downward and cooled. The overall heat transfer characteristics of the enclosure will be described by the average Nusselt numbers, defined as the ratio of the heat flux at the wall if one-dimensional conduction is the only mode of heat transfer.

$$Nu_H = -\frac{(\partial\phi/\partial Y)_{Y=0}}{[1-(1-X_h)Ra_I/Ra_E]} = -\frac{(\partial\phi/\partial Y)_{Y=1}}{[1+X_h Ra_I/Ra_E]}.$$

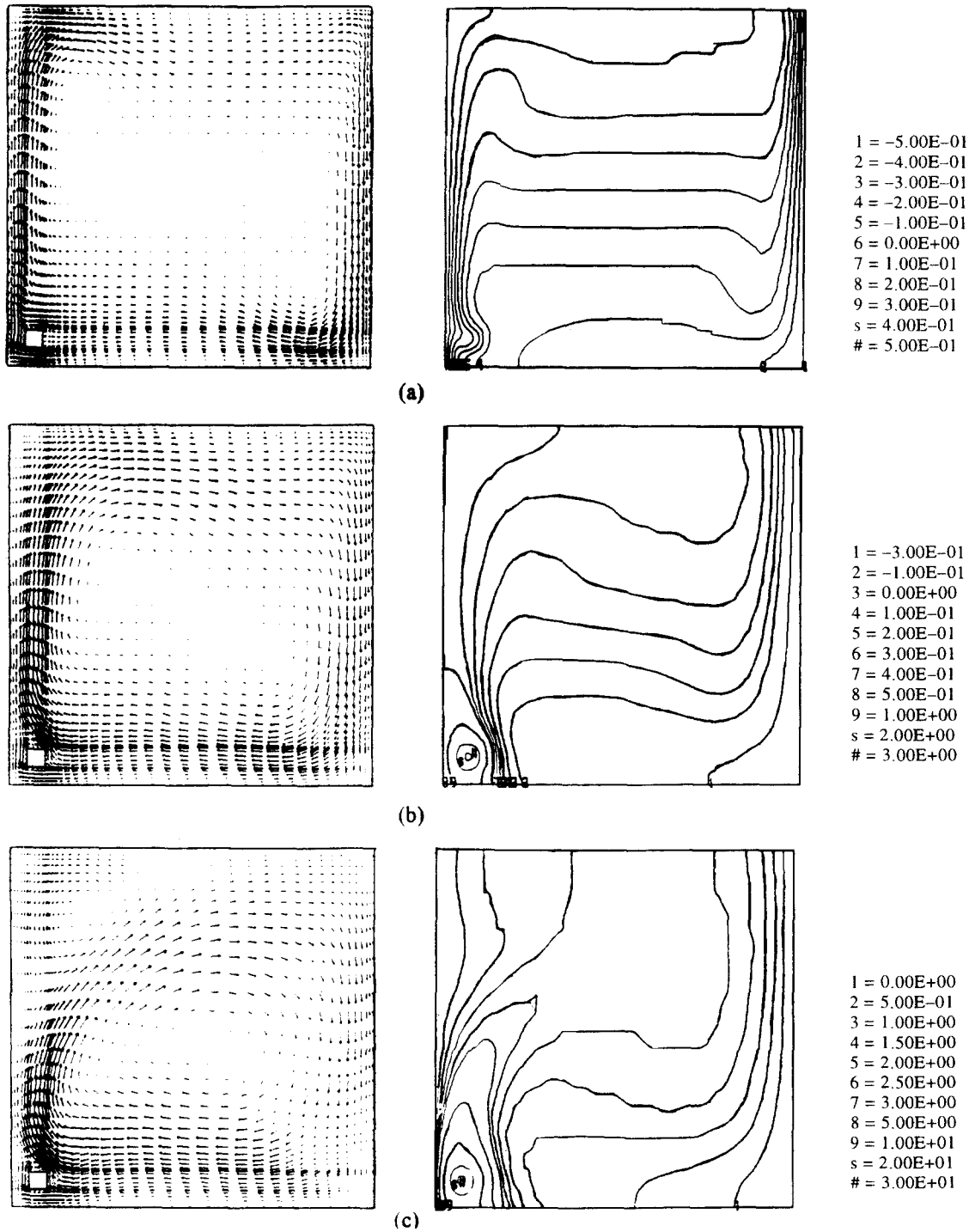

Fig. 3. Velocity patterns and isotherms for $Ra_I = 10^6$ and (a) $Ra_E = 10^6$, (b) $Ra_E = 10^5$, (c) $Ra_E = 10^4$

Based on the above definitions, there is a singularity at $Ra_E = 0.925 Ra_I$ ($X_h = 0.075$) for Nu_H in the geometry considered. At this value, the theoretical conduction heat flux due to the externally imposed temperature difference and the internal heat sources cancel each other. It should be noted that because of this singularity the behavior of the heat flux ratio as defined will be quite irregular in the neighborhood of $Ra_E = 0.925 Ra_I$.

In the absence of an internal energy source, the average heat flux ratio along the hot wall (Nu_H) increases monotonically with Ra_E. The flow adjacent to the hot wall is always upward and the dimensionless temperature gradient at the hot wall is higher than

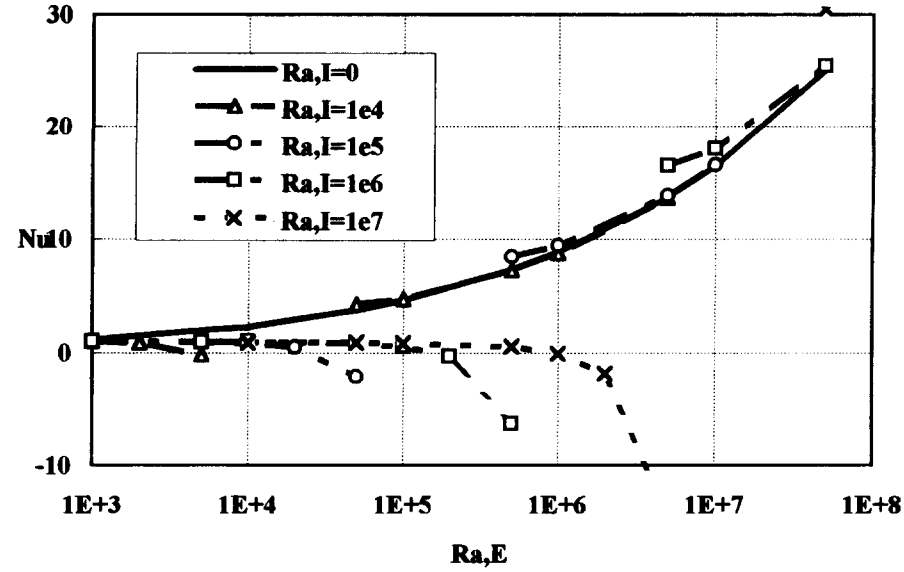

Fig. 4a. Average Nusselt number along the hot wall for cavity flow with an internal heat source.

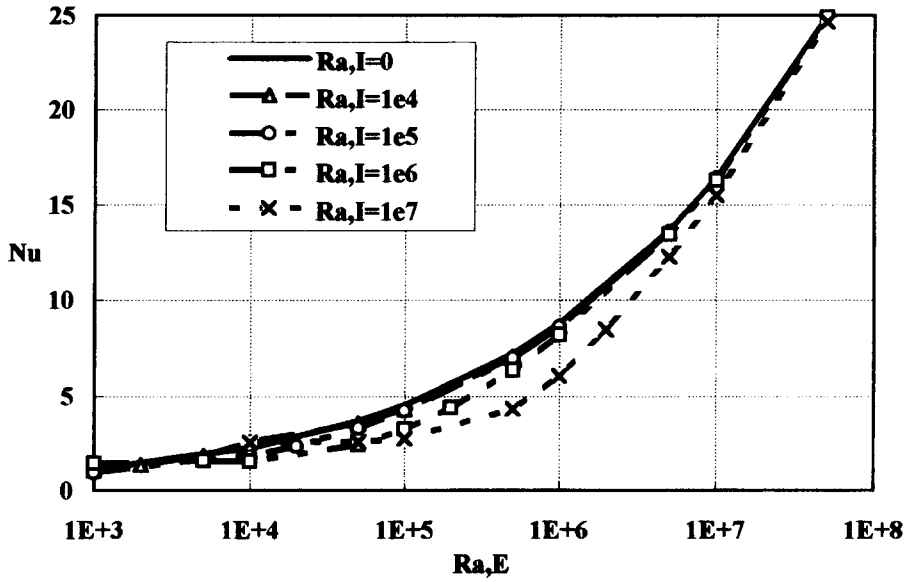

Fig. 4b. Average Nusselt number along the cold wall for cavity flow with an internal heat source.

that of the pure conduction case. In the presence of internal heat sources, the value of Nu_H is governed by the direction and strength of the flow adjacent to the hot wall. At each Ra_I depending on Ra_E, part of the interior hot fluid flows downward along the hot surface forming a counter-direction eddy at the upper corner near the hot wall (Fig. 3c). If Ra_E is increased at each Ra_I, the flow pattern changes from one where the flow adjacent to the hot surface is downward, to one where the flow moves in an upward direction over the surface. In Fig. 4a, the influence of internal energy sources becomes progressively smaller for increasing Ra_E values. In particular, it may be seen that for $Ra_I/Ra_E < 0.1$, the influence of the internal heat source on Nu_H is negligible. For $Ra_I/Ra_E > 100$, the influence of the internal heat source on Nu_H also becomes unremarkable.

Figure 4b shows the variation of the average heat flux ratio (Nu_C) along the cold wall. For all the values of Ra_I, the value of Nu_C increases monotonically with Ra_E because the convective motion always carries heated fluid to the cold wall. For $Ra_I/Ra_E > 1$, the interior temperature is generally smaller than the corresponding conduction temperature since the interior fluid is cooled by the downward flow along the cold wall. Hence, the increase in heat transfer at the cold surface due to the convective motion is offset by the lower interior temperature. Therefore, the corresponding Nu_C are lower than those for the case without internal heaters. For $Ra_I/Ra_E > 100$, the

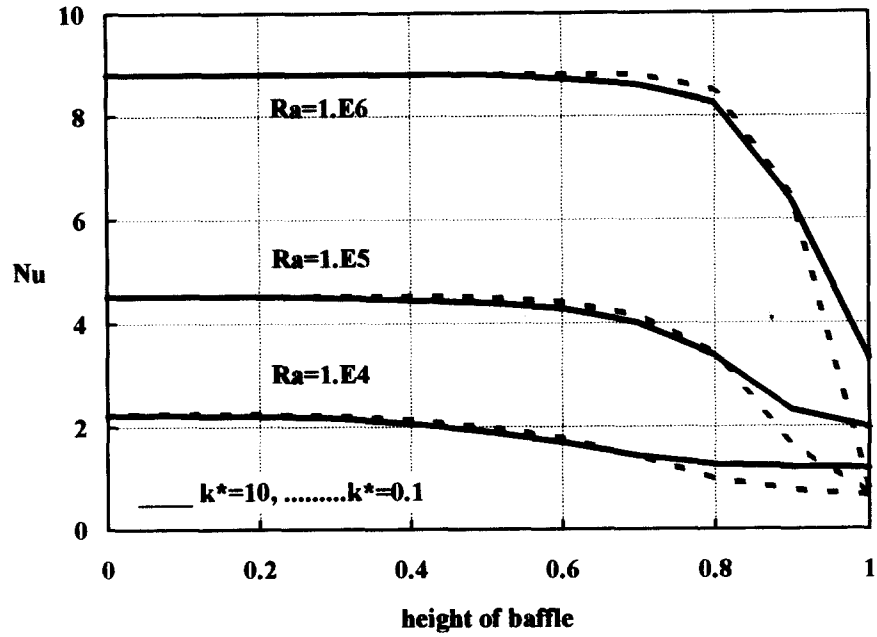

Fig. 5. Influence of baffle height on average Nusselt number for various Ra and k^*. Cavity flow with conductive baffle, without internal heat source.

value of Nu_C approaches a constant for each Ra_I. For $Ra_I/Ra_E < 1$, the external temperature difference dominates the fluid motion. The cold wall receives the fluid directly from the hot wall, so the Nu_C values approach those for the case without internal heat sources.

Effect of conductive baffles

To understand the interactions among the solid baffle, fluid flow and internal heat sources, numerical results have been given by assuming non-conductive walls in Fig. 1.

Sun and Emery [2] examined the effect of a conductive baffle in an enclosure without internal heat sources (Fig. 5). With an increasing baffle height, the driving force for the fluid remains while the resistance to the flow keeps increasing. For a centrally-mounted baffle, as the height of the baffle increases with fixed Ra_E and k^*, the heat transfer decreases. The influence of the increasing baffle height is less important for higher Ra_E, except when the height is so large that the top and bottom ends interfere with the main velocity stream. It also shows that the effect of baffle conductivity on overall heat transfer is very marginal. However, it is noted that for significantly high baffles, the effect of conductivity becomes more obvious and the velocity vectors and isotherms are significantly different for the different conductivities.

In the presence of internal heating ($Ra_I > 0$), the highest temperature occurs near the internal heater. This makes the fluid rise along the hot wall and then turn into the central region of the enclosure. This phenomenon increases the interaction between the baffle and fluid, since the wide stagnation zone in the center of the cavity has been destroyed. Figure 6 shows the average Nusselt number variation on the cold wall. The influence of increasing baffle height is less important for higher Ra_E and smaller Ra_I. This is shown in Fig. 6 by the relative insensitivity of $\overline{Nu}$ to baffle height, and by the similarity to Fig. 5. However, when the internal heating increases and dominates the flow pattern (such as $Ra_E = 10^5$ and $Ra_I = 10^7$), an increase in baffle height significantly affects the heat transfer rate. Figure 7 illustrates that the baffle blocks the flow and forces strong secondary eddies in the hot chamber in the case with higher internal heating. These eddies push warmer fluid through the gap and deliver more heat to the cold chamber ($Ra_E = 10^5$ and $Ra_E/Ra_I = 100$ in Fig. 6). The effect of the centrally-mounted baffle conductivity on heat transfer is very marginal except for high baffles or a high level of internal heating.

It is of interest to understand how the heating ratio affects the average heat transfer. Figure 8 shows the conjugate effect of the heat source ratio and the height of the baffle on the average Nusselt number at a Rayleigh number of 10^5. It shows that, for a small ratio ($Ra_I/Ra_E = 10$ or 15), the presence of a baffle is similar to the case without internal heating—the external Rayleigh number still dominates the flow. Once the ratio increases to $Ra_I/Ra_E = 30$ (a critical value for $Ra_E = 10^5$), the $\overline{Nu}$ is almost a constant no matter what the baffle height is. This critical value is the result of the interaction of the effect of internal heating, baffle height and baffle conductivity. Above the critical ratio, the baffle effect becomes more significant. In Fig. 6, at $Ra_I/Ra_E = 100$ for $Ra_E = 10^6$, the trend is still the same as the case without internal heating.

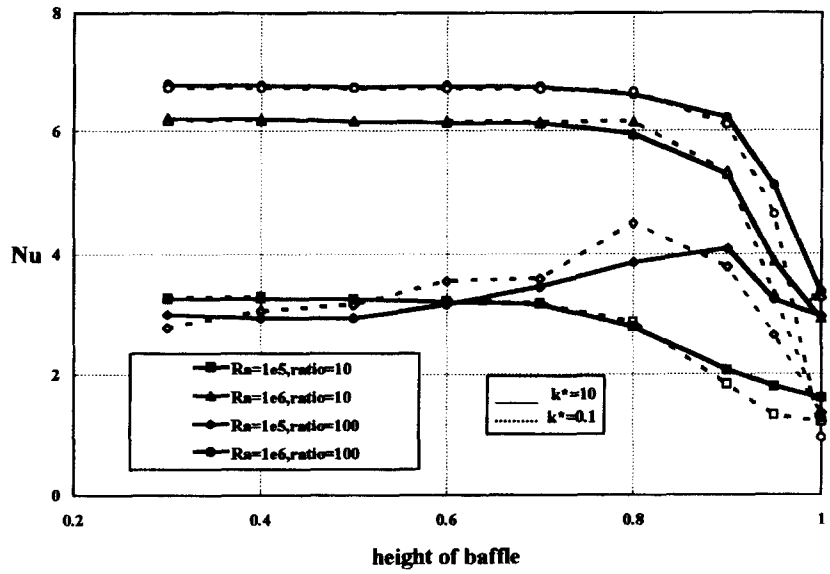

Fig. 6. Influence of baffle height on average Nusselt number for various Ra_E, Ra_I and k^*, where the ratio is Ra_I/Ra_E.

Obviously, the higher the external Rayleigh number, the higher the value of the critical ratio will be.

It is also of interest to observe the effect of baffle when it is located in different locations inside the cavity. For a cavity with a fixed length of baffle ($h_b = 0.9$) and no internal heat source, Fig. 9a ($Ra_E = 10^5$) shows that a conductive baffle increases the overall heat transfer of the enclosure when the baffle is located close to either of the vertical walls, while an adiabatic baffle decreases the heat transfer. For a high Rayleigh number ($Ra_E = 10^6$), the convection totally dominates the fluid flow and a large stagnation zone occurs in the cavity. The effect of baffle location and conductivity is significant only in the boundary layers. In the presence of an internal heat source at the left lower corner of the cavity, the heat source increases the flow strength and almost all the heat transfer is by convection in the fluid instead of conduction through the baffle. Figures 9c and 10b show that the effect of baffle conductivity is negligible in the presence of internal heaters.

COMPARISON OF EXPERIMENTAL DATA WITH PREDICTIONS

Experiments

The experimental apparatus used is part of the HOUSE project at the University of Washington [15]. The special apparatus used, called mimic boxes, are controlled heating calorimeters and are used to measure the window heat flux. Since glazing materials transmit solar radiation and their thermal resistance is small, the technique employed for these measurements is to utilize a calorimeter within a closed box-like construction, one side of which is formed by the window on which the measurements are to be made. A schematic diagram of the mimic box is shown in Fig. 10. The test section is a rectangular box of 57, 20 and 57 cm length, width and height, respectively. The walls are made of 2.54 cm thick styrene foam ($k = 0.32$ W mC^{-1}) on five sides, with the glass window ($k = 1.4$ W mC^{-1}) on the sixth side. There is a baffle located 8.26 cm from the rear, with a 5.08 cm air space at the top and bottom to create a natural convection flow of air washing down over the cold window and up over the heater coil. The baffle is made of 1.27 cm thick styrene foam.

A resistance wire heater heats the box when the inside temperature of the box is lower than the room air temperature outside the mimic box. Since the difference between the temperature inside the mimic box and room temperature is kept small and the styrene foam construction is assumed to be a good thermal resistance, little heat is expected to be lost from the box to the room. Most of the heat lost from the box must then be lost through the window. The mimic boxes measure only the heat lost to the outside, but do not measure any heat gained from the outside. Only night time data are used for this study, so that heat gain from the outside or solar heat gain are not a problem. The heating coil corresponds to a line source of length 2.74 m. Alternating current was supplied to the line source. The voltage rating was measured for each individual mimic box; nominal value was 50 W.

The temperature distributions in the mimic boxes were measured using the two terminal integrated circuit temperature transducers manufactured by Analogy Devices, Inc. and designated as AD590s. The locations of the AD590s are provided in Fig. 11a.

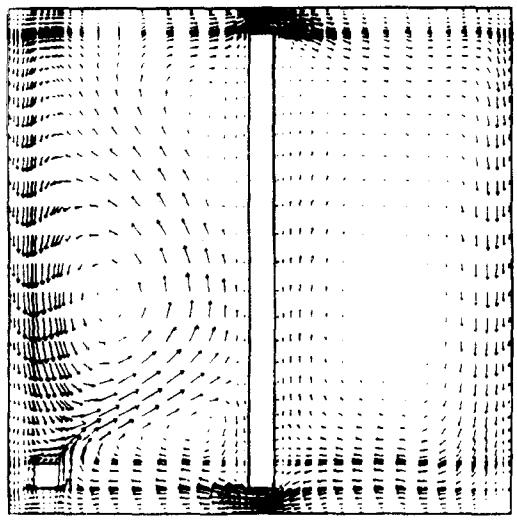

(a)

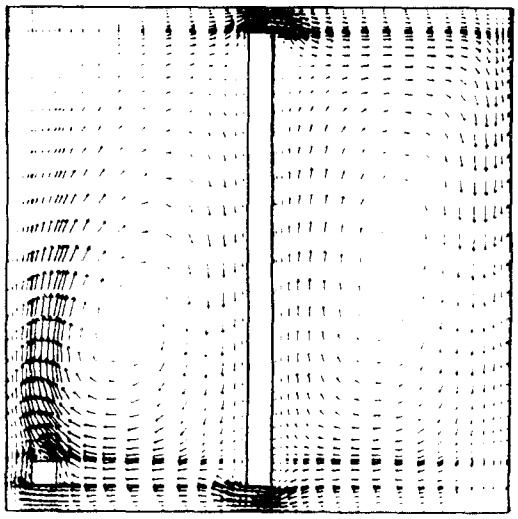

(b)

Fig. 7. Velocity patterns for $Ra_L = 10^5$ and (a) $Ra_I = 10^7$, (b) $Ra_I = 10^6$.

The AD590s were positioned approximately 4.13 cm behind the glass pane. The indoor and outdoor temperatures were not controlled, but were allowed to vary with the environment. The indoor temperature was maintained at a nearly constant value by use of a thermostat, while the outdoor temperature depends totally upon the weather conditions.

Comparison of experimental data with predictions

To find the two-dimensional natural convection at the central plane, the mimic box is simulated as a rectangular cavity with an aspect ratio of 2.86, conductive walls and baffles, and three internal heat sources—two in the lower cavity and one in the upper cavity, all located behind the baffle. The average values of the dynamic temperature measurements are assumed to approximate steady state results. The oscillation of the measured temperature data shows that these average values have a maximum error of 1.5°C. A large temperature difference was found between the inside glass surface and the outdoor environment [14]. Different temperatures are measured at the glass surface and obviously the outdoor temperature cannot be used as a constant temperature boundary condition. Instead, a simulation of heat transfer through the exterior air film and the glass itself is needed. The exterior air film is assumed to be a solid zone, as is the glass, but with the conductivity based on the free convection heat transfer coefficient and thickness of the air layer. This idealized boundary condition does not give the exact temperature profile on the surface of the glass, but this method does give a reasonable temperature profile on the cold surface of the cavity. An example of the comparison between the measured temperatures and predicted values on the glass surface is shown in Fig. 12a. Since the exterior condition is not measured, variable trial and error processes are used to give an approximation to the measured surface temperatures. Even though the measured surface temperatures are not very accurate due to the difficulty of attaching sensors onto the surface, the approximation is more reasonable than the use of constant outdoor temperature.

A sample of resulting comparisons is shown in Fig. 12b. Note that there are very large deviations between the measurements and numerical predictions using the outdoor temperature as the boundary condition of the cavity (without the simulation of exterior air layer), but the numerical results are improved by simulating the exterior air layer as a solid wall with effective conductivity. The agreement between the improved prediction and measurement is good. The deviation is primarily due to the boundary condition modeling approximations at the glass surface. The velocity vector patterns and isotherms are shown in Fig. 11b and c. Temperature stratification in front of the baffle shows that the baffle successfully creates a natural convection flow in the frontal cavity, except in the regions near the top and bottom.

The differences between the predictions and measurements are the net result of several factors: such as the three-dimensional effect, the effect of radiation, the effect of the edge and frame of the window, the exterior forced convection due to the wind, the dynamic weather conditions, the temperature stratification on the vertical walls, the imperfection of the insulation at the horizontal walls, the difficulty of holding the temperature sensors in the air and the uncertainties in thermophysical properties etc.

Several test nights with various temperature differences are examined (Table 1). The temperature differ-

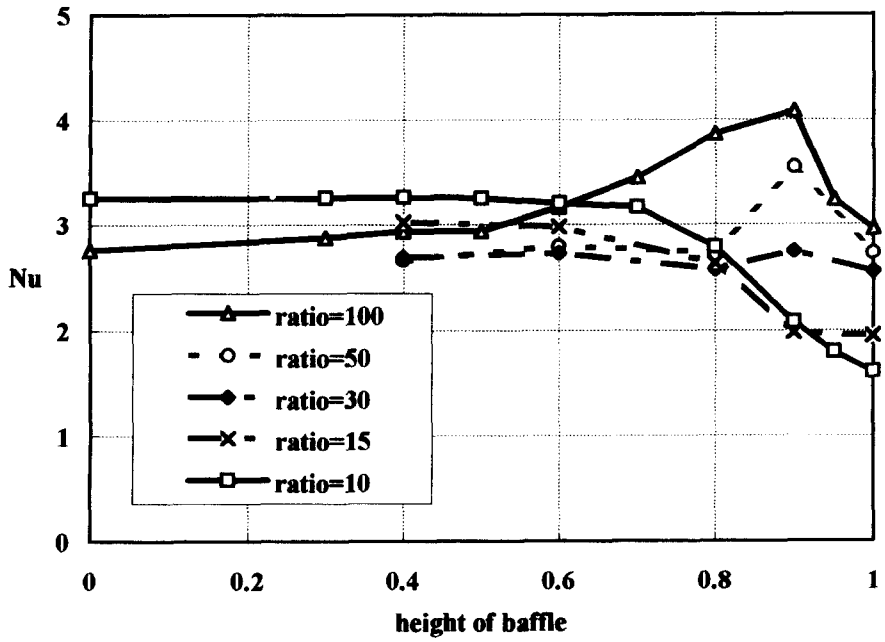

Fig. 8. Effect of heating ratio on the average Nusselt number (cold wall) at $Ra_E = 10^5$.

ence from 10 to 25°C causes the external driving force equivalent to Ra_E from 5×10^7 to 5×10^8 and the ratio of internal–external heating (Ra_I/Ra_E) from 5.5 to 7.5. It is noted that a large percentage of heat loss (η) is contributed by the hot wall, not only from the heaters as assumed. This result indicates that the conduction of the cavity walls is not negligible. However, the percentage of heat loss through the hot wall is in the range 33–40% based on the range of temperature differences. This might be used to correct the present calculation of window U-values by replacing Q with q_C ($=Q/1-\eta$).

CONCLUSIONS

The qualitative and quantitative understanding of the influences of conjugate conduction–convection heat exchange and internal–external heating are presented in this study. When internal heating is used inside the cavity, variations of the numerical solution from the benchmark solution (without internal heat sources) show up only when the heating ratio (Ra_I/Ra_E) is in the range of 1–10. For a ratio less than 1, internal heating does not affect the flow pattern and heat transfer, and the external temperature difference is still dominant. For a ratio greater than 10, the average Nusselt number tends to reach a constant value.

When using conductive walls, the average Nusselt number is found to increase when the conductivity ratio (solid–fluid) increases. The effects of the void fraction depend on the conductivity of the wall material. For low conductivity walls, an increase in void fraction increases the heat transfer. For high conductivity walls, the average Nusselt number decreases with an increase in void fraction.

For an enclosure with a conductive baffle, results indicate that heat transfer is strongly influenced by the coupling effect among baffle conduction, fluid convection and the strength of internal heating when the baffle is located near walls. The increasing resistance to the fluid due to the baffle decreases the overall heat transfer. When the baffle is conductive, heat can still be transferred to the rest of the enclosure by conduction. When the baffle is adiabatic or when the convection dominates the flow due to a high level of internal heating, heat is transferred by convection no matter what the value of the baffle conductivity. The influence of the baffle become marginal when it is located centrally, since it then sits in a wide stagnation zone in the center of the cavity for higher Ra flow.

A practical window calorimeter is simulated as a parametric study. Qualitative agreement has been found between the simulations and measurements. In quantitative comparison, deviations were generated due to uncontrollable and dynamic boundary conditions. By modifying the simulation of the exterior air film and glass pane, better boundary conditions (temperature profiles) have been derived, and the deviations have been reduced to less than 25%. The 25% maximum relative error is quite good considering the many factors which affect the accuracy of the experiment. Calculation of the window U-value should be corrected by considering the heat loss through the walls, but it is not practical to actually calculate the amount of heat loss for each case. The

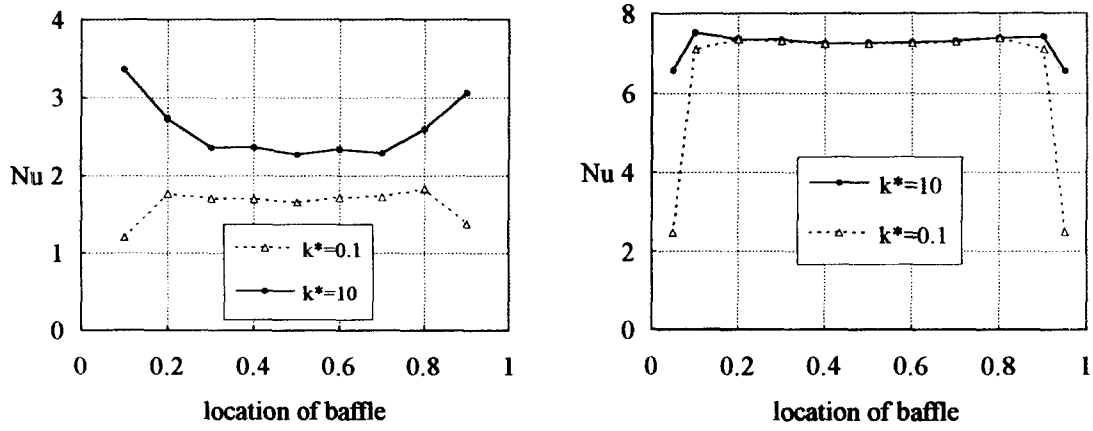

(a) without internal heat source, $Ra_E = 10^5$ (left), $Ra_E = 10^6$ (right)

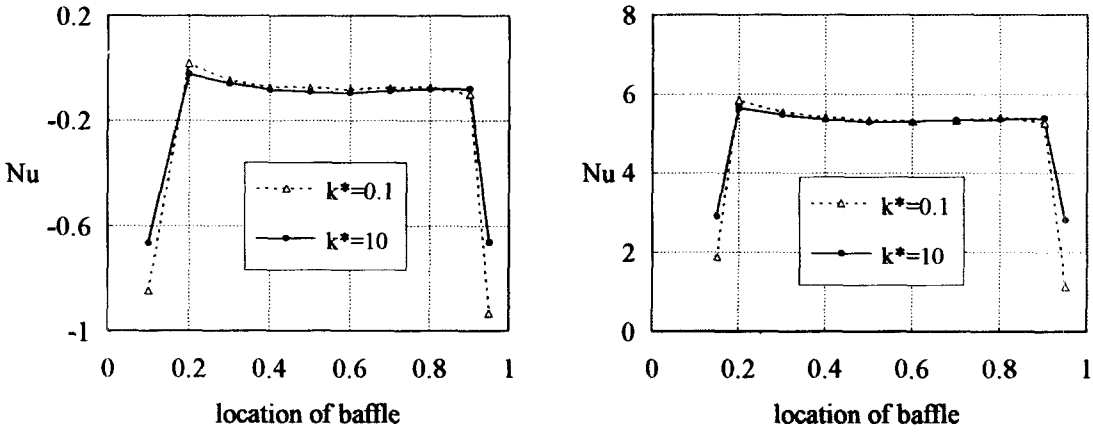

(b) low level of internal heating, $Ra_E = 10^6$, Ra_I/Ra_E=10, left(hot wall), right (cold wall)

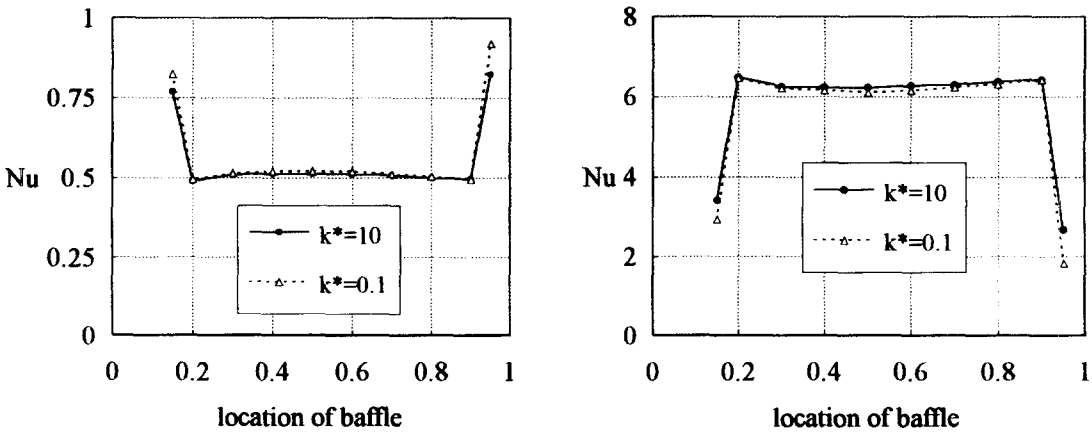

(c) high level of internal heating, $Ra_E = 10^6$, Ra_I/Ra_E=100, left(hot wall), right (cold wall)

Fig. 9. Effect of baffle locations on the average Nusselt number, with $h_b = 0.9$.

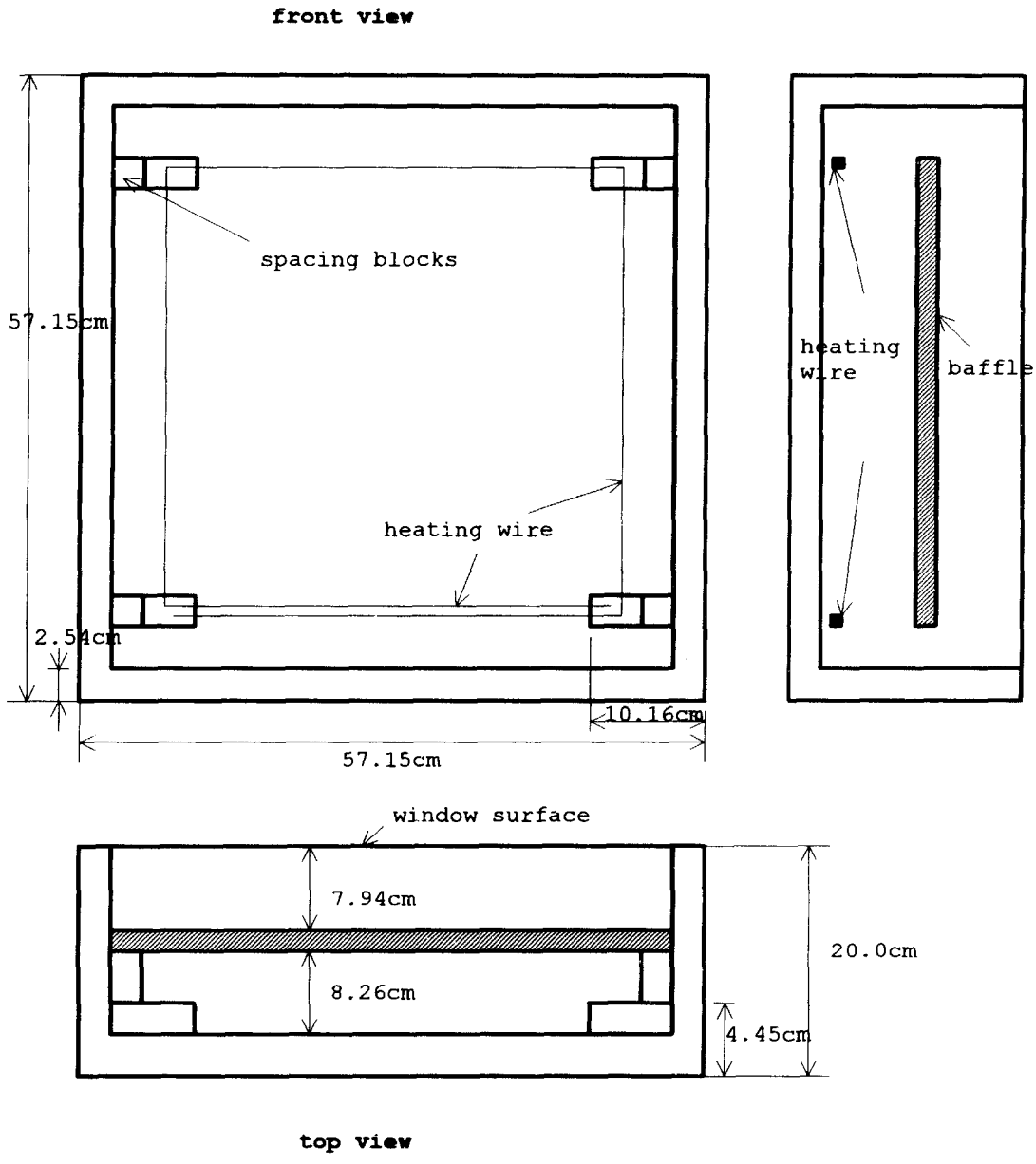

Fig. 10. Schematic diagram of mimic box.

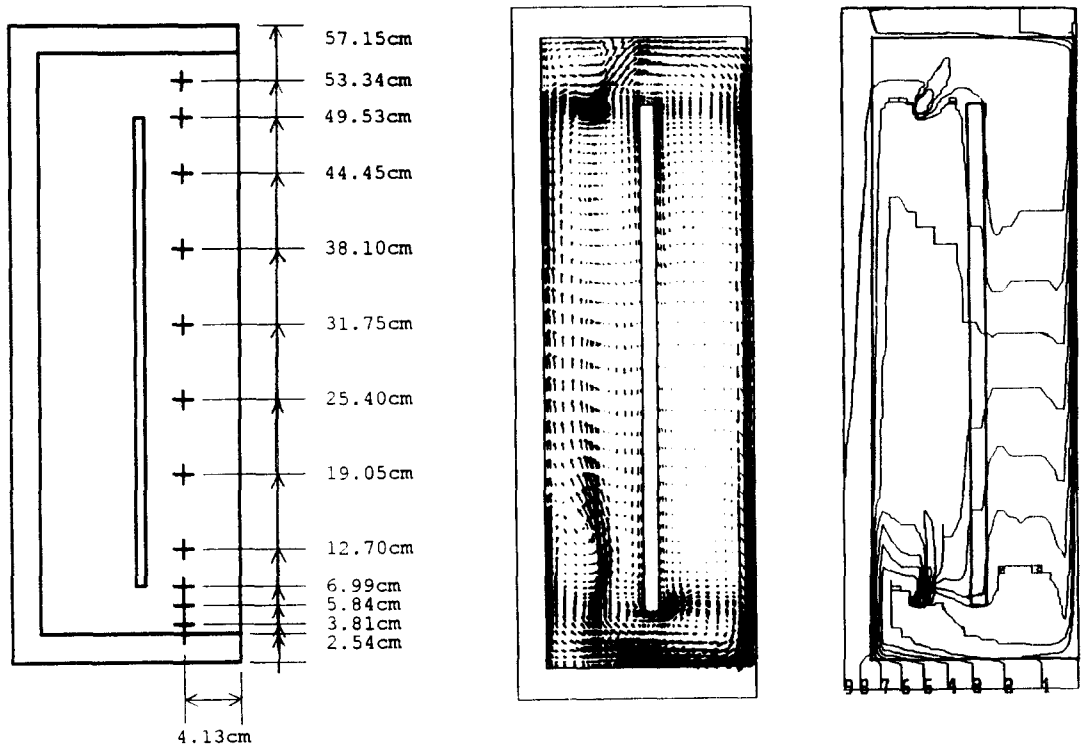

Fig. 11. Locations of temperature sensors (a), sample of a velocity pattern (b) and (c) isotherms of mimic box (window calorimeter).

Table 1. Results of numerical simulation of window calorimeter

	1	2	3	4	5
T_H [C]	22.17	20.02	20.51	25.03	19.64
T_C [C]	1.66	0.14	7.51	0.00	7.06
ΔT [C]	20.51	19.88	13.00	25.03	12.58
Ra_E ($\times 10^{-8}$)	3.346	4.505	0.64	5.4	3.83
Ra_i/Ra_E	5.519	6.532	5.813	7.268	5.884
k^*	12.698	12.78	12.55	12.76	12.74
q_H	8.272	11.244	11.901	13.475	10.702
q_C	24.83	30.84	29.34	35.279	28.234
η (%)	33.3	36.46	40.56	38.2	37.9

$q_H = -\partial\theta/\partial y$ at the hot wall, positive to the exterior.
$q_C = -\partial\theta/\partial Y$ at the cold wall, positive to the exterior.

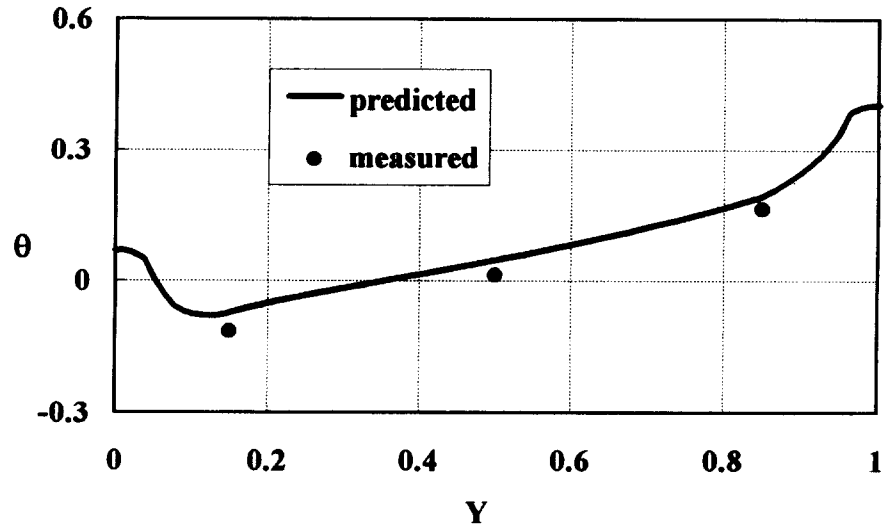

(a)

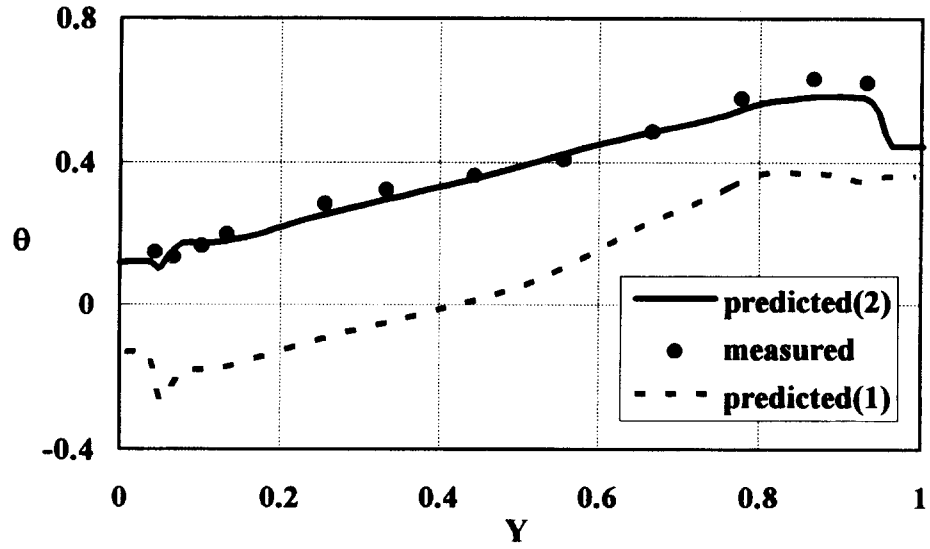

(b)

Fig. 12. Comparison of predicted and measured data with T_H = 20C, T_C = 2C and ΔT = 18c. (a) Temperature profile on a glass surface, (b) temperature profile inside the cavity: predicted data (1) without, (2) with air layer simulation.

range of heat loss percentage (η) given by the present investigation might be valuable for present parametric cases.

REFERENCES

1. M. W. Wong, An experimental study of window management of nine different types of window products. M.Sc. Thesis, Department of Mechanical Engineering, University of Washington, Seattle, WA (1990).
2. Y. S. Sun and A. F. Emery, Multigrid computation of natural convection in enclosures with a conductive baffle, *Numer. Heat Transfer* **25**, 575–592 (1994).
3. G. de Vahl Davis, Natural convection of air in a square cavity : a bench mark numerical solution, *Int. J. Numer. Meth. Fluid* **3**, 249–264 (1983).
4. D. R. Chenoweth and S. Paolucci, Natural convection in an enclosed vertical air layer with large horizontal temperature differences *J. Fluid Mech.* **169**, 173–210 (1986).
5. R. A. W. M. Henks and C. J. Hoogendoorn, On the stability of the natural convection flow in a square cavity heated from the side, *Appl. Sci Res.* **47**, 195–220 (1990).

6. F. P. Incropera, Convection heat transfer in electronic equipment cooling, *J. Heat Transfer* **110,** 1097–1111 (1988).
7. S. Acharya and R. J. Goldstein, Natural convection in an externally heated vertical or inclined square box containing internal energy sources, *J. Heat Transfer* **107,** 855–866 (1985).
8. J. Davalath and Y. Bayazitoglu, Forced convection cooling across rectangular blocks, *J. Heat Transfer* **109,** 321–328 (1987).
9. M. Afrid, and A. Zebib, Natural convection air cooling of heated components mounted on a vertical wall, *Numer. Heat Transfer* **15,** 243–259 (1989).
10. Y. Joshi, L. O. Haukenes and S. B. Sathe, Natural convection liquid immersion cooling of a heat source flush mounted on a conducting substrate in a square enclosure, *Int. J. Heat Mass Transfer* **36,** 249–263 (1993).
11. D. M. Kim and R. Viskanta, Effect of wall heat conductance on natural convection heat transfer in a square cavity, *J. Heat Transfer* **107,** 139–146 (1985).
12. S. V. Patankar, *Numerical Heat Transfer and Fluid Mechanics*. Hemisphere, Washington, DC (1980).
13. A. Pollard and A. L. Siu, The calculation of some laminar flows using various discretisation schemes, *Comput. Meth. Appl. Mech. Engng* **35,** 293–313 (1982).
14. Y. S. Sun, Conjugate natural convection heat transfer in a rectangular cavity containing internal heat sources. Ph.D. thesis, Department of Mechanical Engineering, University of Washington, Seattle, WA (1994).
15. A. F. Emery, C. J. Kippenhan, G. B. Varey, J. L. Garbini, J. H. Heerwagen and D. R. Heerwagen, *The Thermal Interaction of Envelope Components in Standard and Improved Houses in the Pacific Northwest*, HTD-Vol. 123, pp. 153–162. ASME, New York (1989).